Molecular stabilization of chemically exfoliated bare $MnPS_3$ layers

Isaac Brotons-Alcázar,[a] Ramón Torres-Cavanillas [a] Marc Morant-Giner,[a] Martin Cvikl,[a] Samuel Mañas-Valero,[a] Alicia Forment-Aliaga*[a] and Eugenio Coronado.*[a]

Transition metal chalcogenophosphates of general formula MPX_3 have attracted recent interest in the field of 2D materials due to the possibility of tuning their properties when reaching the 2D limit. Several works address this challenge by dry mechanical exfoliation. However, only a few of them use a scalable approach. In this work, we apply a general chemical protocol to exfoliate $MnPS_3$. The method uses in a first step chemical intercalation and liquid phase exfoliation, followed in a second step by the addition of molecules used as capping agents on the inorganic layers. Therefore, molecules of different nature prompts the quality of the exfoliated material and its stabilization in aqueous solution, opening the possibility of using these functionalized layers in several fields. Here we illustrate this possibility in electrochemistry. Thus, we show that when polyethylenimine is used as capping agent, it is possible to reach a compromise between the stability of high quality $MnPS_3$ flakes in aqueous suspension and their optimum performance as an electrocatalytic system for HER activity.

Introduction

Among the many materials with a 2D structure, the family of transition metal chalcogenophosphates (MPX_3; where M = V, Cr, Mn, Fe, Co, Ni, Cu, Zn and Cd and X = S, Se, Te) has recently attracted the growing attention of the research community.[1] This interest arises from its extensive variety of electronic and magnetic properties.[2,3] Thus, for example, these materials exhibit a wide bandgap (up to 3.5 eV)[4] that broaden their potential application in optoelectronics;[5] In addition, these materials exhibit cooperative magnetic properties, in particular antiferromagnetism,[6] which has been proven to persist even in the 2D limit.[7,8] Interestingly, the reliance between structural, electronic and magnetic properties boosts their potential in spintronics.[6] Furthermore, these materials have also been studied as promising candidates for electrocatalytic applications.[9]

Notice that most of the works focused on the fundamental characterization of ultrathin layers use dry approaches to obtain these layers, either top-down, using the scotch-tape method for exfoliating large crystals,[10] or bottom-up strategies for synthesizing nanosheets in a controlled way.[11] These methods give rise to high quality single or few layers MPX_3 with a low degree of defects. However, for large-scale applications they suffer from an important lack of scalability. From a different point of view, we find methods in solution, like bottom-up chemical synthesis from thiohypophosphate $(P_2S_6)^{4-}$ anions and divalent metallic cations M^{2+},[12] and the top-down liquid-phase exfoliation (LPE) approach. These strategies provide much higher versatility and processability, making them perfect candidates for developing 2D-crystal-based functional inks.[13,14] Regarding LPE approach, it is a straightforward method but with a low degree of control over the quality of the layers. Even so, very few works have tried to exfoliate MPX_3 through sonication-assisted exfoliation. This method has permitted to improve, for example, the electrocatalytic activity of these nanosheets with respect to the bulk.[15] Unfortunately, the thickness and the lateral dimension of the resulting flakes are not of the finest quality.[15,16] In order to improve the quality of the flakes, we can benefit from the well-known capacity of MPX_3 family to chemically intercalate ions in between their layers[17] to expand them before the sonication step. This ability was first applied by Frindt et al.[18] to exfoliate $MnPS_3$ and $CdPS_3$. However, full characterization of the resulting layers was not reported, and it was mandatory to use polyvinylpyrrolidone (PVP) as a capping agent to achieve the exfoliation of $MnPS_3$.

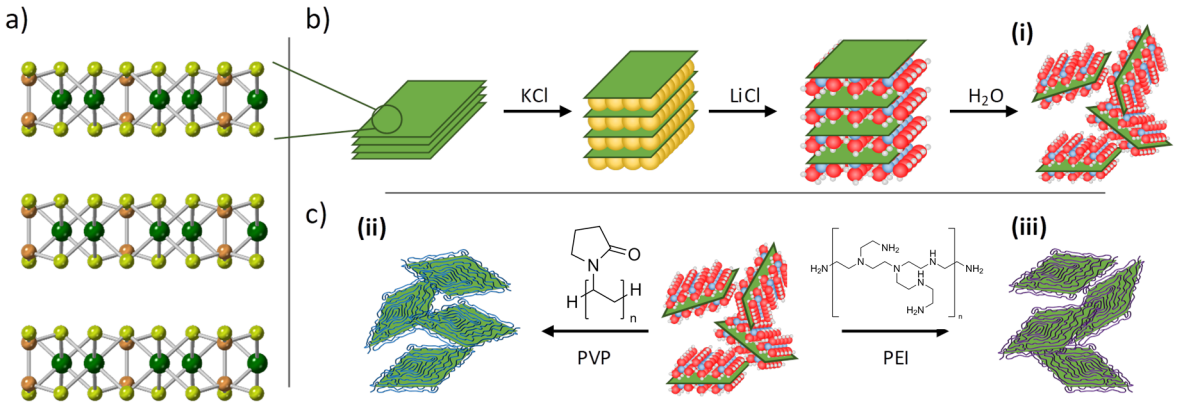

Scheme 1 Structure, intercalation and exfoliation protocol of $MnPS_3$. a) Crystalline structure of three stacked $MnPS_3$ layers (S: Yellow; Mn: Green; P: Orange). Each layer is represented by a green sheet in (b) and (c). b) Double step K^+, Li^+ intercalation process giving rise to $MnPS_3@H_2O$ (i) suspended layers through final sonication step. c) Once $MnPS_3@H_2O$ dispersion is obtained the addition of PVP or PEI aqueous solutions permit the incorporation of the capping agents around the flakes and $MnPS_3@PVP$ (ii) or $MnPS_3@PEI$ (iii) suspensions are formed.

Notice that the presence of a capping agent can be either beneficial or detrimental.[19] On the beneficial side, it can stabilize the sheets, improve the dispersion in different solvents or facilitate their functionalization with active functional groups. However, its presence can be detrimental for applications involving the accessibility of species to the surface of the nanosheet since it can be hindered.[20] In this scenario and focusing on $MnPS_3$ as a prototype MPX_3 material, we have optimized the previously reported chemical intercalation-exfoliation process to obtain aqueous suspensions of high-quality layers with and without the use of different capping agents (see Scheme. 1). Herein we present a detailed study of the stability of the suspensions and the quality of the resulting layers. In a further step, we have proved how, by means of choosing an optimum capping agent, it is possible to obtain a compromise between suspension stability and high accessibility to the $MnPS_3$ surface, fostering its applicability in fields like electrocatalysis in which the solution/solid interface is key.

Results and discussion

Bulk crystalline $MnPS_3$ was prepared performing a solid-state reaction[2] and exfoliated through chemical intercalation in two steps with K^+ and Li^+ ions.[18] Furtherly, the obtained material was exfoliated through probe assisted sonication. The so obtained material was resuspended in water ($MnPS_3@H_2O$) in order to obtain a 2D ink of fully accessible flakes. Alternatively, two different capping agents were added, i.e.: polyvinylpyrrolidone (PVP)[21] and polyethylenimine (PEI),[22] being both well-known capping agents for stabilizing nanomaterials in aqueous solutions. The use of these polymers gave rise to $MnPS_3$@PVP and $MnPS_3$@PEI suspensions, respectively. These three systems were fully characterized and compared with each other.

Structural and chemical characterization

Once the suspensions were obtained, the drying of the flakes as solids was mandatory in order to perform solid-state characterization measurements. With this goal, all suspensions were centrifuged and the resulting solid was extensively purified by three redispersion in water and centrifugation cycles. This step is decisive to remove any excess of the intercalation ions or polymers not attached to the $MnPS_3$ layers.

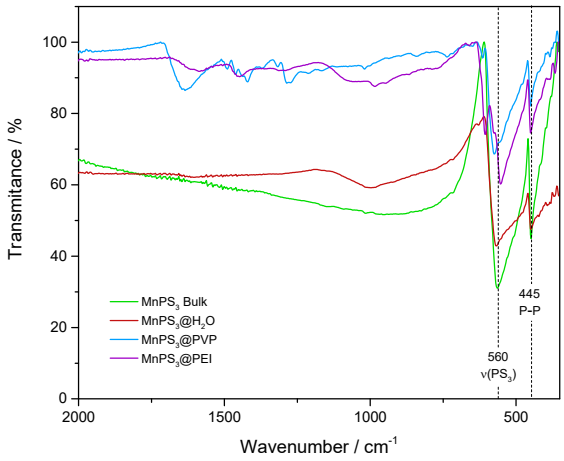

Fig. 1 Low energy region of the ATR-IR spectra of bulk $MnPS_3$ (green), $MnPS_3@H_2O$ (red), $MnPS_3$@PVP (blue) and $MnPS_3$@PEI (purple) powder samples.

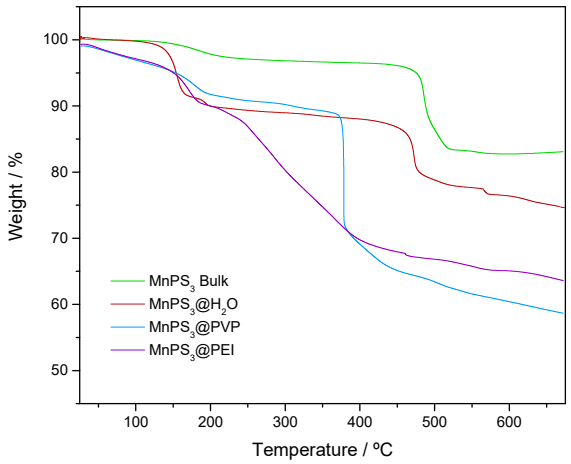

Fig. 2 TGA analysis under N_2 atmosphere of bulk $MnPS_3$ (green), $MnPS_3@H_2O$ (red), $MnPS_3$@PVP (blue) and $MnPS_3$@PEI (purple) powder samples.

Attenuated total reflection infrared spectroscopy (ATR-IR). Infrared spectroscopy, provided information first, on the presence of the organic capping in the protected samples and, second, about the chemical stability and perturbations of $MnPS_3$ after the intercalation/exfoliation process. This last aspect was furtherly supported by Raman spectroscopy (see ESI Fig. S1). As can be seen in ESI, Fig. S2 and Fig. S3, the high energy region of the IR spectra gives evidence of the polymeric capping agents in the composite like the carbonyl vibration in $MnPS_3$@PVP and amino vibration in $MnPS_3$@PEI. Focusing on the low energy region of the IR spectra Fig. 1 (~800-400 cm^{-1} range), specific information of the inorganic layers can be extracted. Thus, in $MnPS_3$ bulk sample it is possible to distinguish two characteristic bands. The first one appears at 445 cm^{-1} and corresponds to P—P vibration. The second one corresponds to asymmetric stretching $\nu(PS_3)$ and is centered at 560 cm^{-1}. An analogous spectrum is recorded for $MnPS_3@H_2O$ but a different behaviour is observed for $MnPS_3$@PVP and $MnPS_3$@PEI. In these last cases, we notice a clear splitting of the asymmetric stretching $\nu(PS_3)$ band in $MnPS_3$@PEI, which is less intense but is also present in $MnPS_3$@PVP. A similar splitting of the $\nu(PS_3)$ band was previously reported by Clément and coworkers[17] in the infrared spectra of $MnPS_3$ Li^+ intercalates. This splitting was attributed to the creation of metallic Mn vacancies in the layer since this deffects give rise to inequivalent P—S bonds (because some S atoms are coordinated to Mn centres, while others are not). However, in our systems, XPS measurements confirm that we do not have a high number of Mn

defects and that we successfully removed all the intercalated Li^+ ions (that could compensate Mn vacancies), see ESI Fig. S4-S6. Therefore, the reason behind the splitting detected in the composites should be the interaction with the polymeric capping layers. In $MnPS_3$@PEI, PEI has primary, secondary, and tertiary amino groups, probably protonated at pH = 5 in the $MnPS_3$@H_2O suspension where PEI is added. These groups can interact with some of the P_2S_6 bipyramids through sulfur electron pairs, distorting their vibration, affecting the ν(PS_3) signal and the characteristic amine bands (ESI Fig. S3). In the $MnPS_3$@PVP this capping agent is not expected to present an effective interaction with the nonbonding S electrons. However, it may be able to interact with metallic atoms through the carbonyl groups present. Such interaction is confirmed by the red-shift observed for the carbonyl band of the PVP[23] from 1644 cm^{-1} to 1632 cm^{-1} (Fig. S2). This interaction could indirectly affect Mn—S bonds and as a result, the P—S stretching.

Thermogravimetric analysis (TGA). For estimating the thermal stability of the systems and the amount of capping agent present in our samples, TGA were carried out under inert atmosphere. Bare $MnPS_3$ in bulk form and both capping agents were analysed by this technique and used as reference samples (Fig. 2 and ESI Fig. S7). Afterwards, the $MnPS_3$@H_2O, $MnPS_3$@PVP and $MnPS_3$@PEI systems were evaluated under the same experimental conditions Fig. 2. From room temperature until 200 ºC weight losses in all samples are related to absorbed water, which is significantly larger in exfoliated systems due to occluded water molecules between the layers.[24] Upon a further increas of the temperature, bulk $MnPS_3$ does not suffer any significant weight loss until ~480ºC when the inorganic solid starts its decomposition that takes place in the 480-515ºC range. This drop is shifted between 460-485ºC when the material is exfoliated. However, $MnPS_3$@PVP presents a sharp weight loss at ~375ºC very similar to the one observed in the TGA of pure PVP (ESI Fig. S7), while $MnPS_3$@PEI shows a first small continuous decrease between 180-250ºC and a second larger one, but also very gradual, between ~250-450ºC, that contrast with the sharp single step observed at ~320ºC for pure PEI (ESI Fig. S7). These results support the presence of the organic polymers in the composites once more and evidence the existence of stronger interactions between PEI and the inorganic flakes than for PVP. In more detail, the first gradual thermal decomposition of $MnPS_3$@PEI (~180-250ºC range) seems to point out to a small amount of physisorbed PEI, while the second (~250-450ºC range) supports the presence of a significant amount of PEI strongly interacting with the inorganic layers probably due to the presence of positively charged amino groups of the polymer interacting with S atoms of the flake. Similar trends have been observed in PEI wrapped graphene oxide layers.[25] Finally, for the calculation of the polymeric content, it is important to consider that from 400ºC, there is an overlap between polymer and $MnPS_3$ decomposition. In order to avoid the overestimation of the polymeric content in the hybrid systems, we have considered a 17% weight loss at 675ºC, strictly related to the degradation of the inorganic exfoliated material, once H_2O content has been already eliminated below 200ºC (Calculated from $MnPS_3$@H_2O TGA, Fig. 2). Taking all these considerations, a ~21% and a ~14% of polymer content is assessed for $MnPS_3$@PVP and $MnPS_3$@PEI, respectively. A summary of the water and polymer percentages in all samples is presented in Table 1.

Table 1 Percentages of $MnPS_3$, capping agent and water for each system determined by TGA analysis

System	$MnPS_3$ / %	H_2O / %	Capping agent / %
$MnPS_3$ Bulk	98.0	2.0	-
$MnPS_3$@H_2O	90.0	10.0	-
$MnPS_3$@PVP	70.5	8.3	21.2
$MnPS_3$@PEI	76.5	10.0	13.5

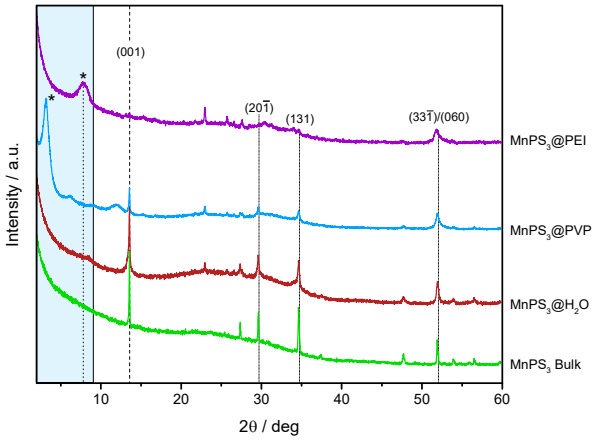

Fig. 1 PXRD patterns of bulk $MnPS_3$ (green), $MnPS_3$@H_2O (red), $MnPS_3$@PVP (blue) and $MnPS_3$@PEI (purple) powder samples measured in capillary.

X-ray powder diffraction (XRPD). Crystallinity of the samples was investigated through XRPD. Diffraction patterns of the exfoliated samples resemble that of bulk $MnPS_3$ (Fig. 3), denoting that main crystalline structure is preserved. Peak (001) at $2\theta = 13.6^{o}$ corresponding to an interlayer distance of d=0.65 nm in bulk $MnPS_3$, is maintained unaltered in $MnPS_3@H_2O$ but a clear broadening indicates a drop in the periodicity along the c-axis, which is due to the decrease in the number of stacked layers. However, new diffraction peaks emerge at lower angles once the material is wrapped by the organic polymers (highlighted area in Fig. 3). These new peaks are related to new interlayer spacing for the slabs of $MnPS_3$.[26] Thus, in the case of $MnPS_3$@PEI, the main peak appears at $2\theta = 7.8^{o}$ corresponding to an interlayer spacing of 1.14 nm and in the case of $MnPS_3$@PVP at $2\theta = 3.22^{o}$ indicating a new interlayer distance of 2.74 nm. As these polymers can be arranged in different ways around the flakes, more than one peak can appear sometimes as observed for PVP. However, their intensities are much lower than those just mentioned, suggesting a main preferential ordering between the layers driven by the intense interaction between the capping agents and $MnPS_3$ layers, as was deduced by the IR spectra. It is important to mention that the assignment of these low angle diffraction peaks to K^+ or Li^+ intercalated $MnPS_3$ can be excluded by the measurement of the corresponding diffraction patterns of these intercalated systems. (ESI Fig. S8)

Morphological characterization

After finishing the exfoliation procedure, the obtained suspensions were spin-coated on Si/SiO_2 substrates for their further morphological characterization.

Atomic force microscopy measurements. The deposited layers were analysed by AFM to study their size and shape. Topography

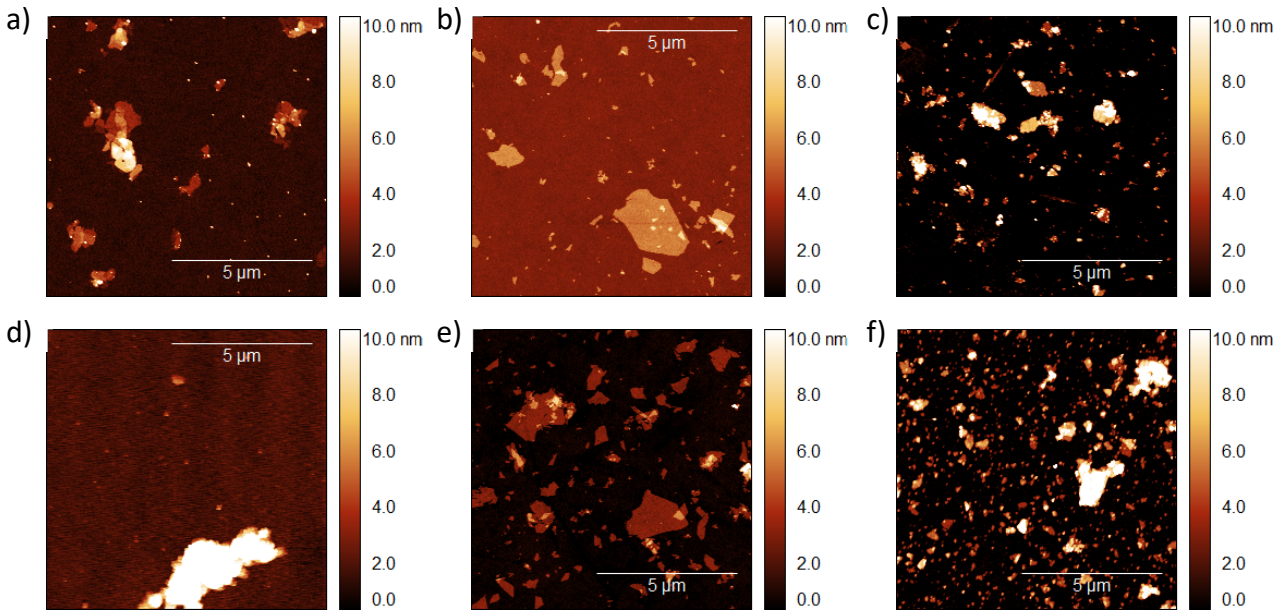

Fig. 2 Top: AFM topography images of $MnPS_3@H_2O$ (a), $MnPS_3$@PVP (b) and $MnPS_3$@PEI (c) spin-coated on Si/SiO_2 substrates right after suspensions were prepared (day 1). Bottom: AFM topography images of $MnPS_3@H_2O$ (d), $MnPS_3$@PVP (e) and $MnPS_3$@PEI (f) spin-coated on Si/SiO_2 substrates five days after suspensions used in top images, were prepared (day 5).

images in Fig. 4 (a-c) show flakes obtained from freshly prepared $MnPS_3@H_2O$, $MnPS_3$@PVP and $MnPS_3$@PEI suspensions. In all cases, the images present homogeneous high-quality flakes with larger areas and lower thicknesses than those previously reported using pure sonicated-assisted approach, without preliminary intercalation.[16] Moreover, analysing the height profiles of the flakes in detail, we find ~1 nm thick $MnPS_3$ bare flakes from $MnPS_3@H_2O$ suspension, what means that our exfoliation has arrived to the monolayer limit. However, in the case of $MnPS_3$@PVP and $MnPS_3$@PEI, higher thicknesses are observed. As the exfoliating procedure is the same for all the samples, this difference should be related to the organic component. In order to get a better interpretation of these results, we studied the height histograms extracted from the AFM pictures of each system Fig. 5 and Fig. S10-S11. This analysis clearly indicates that while bare $MnPS_3$ flakes only show maxima at 1 nm and multiples of 1 nm, this is not the case for $MnPS_3$@PVP where we detect maxima at ~2.8 nm and their multiples. This periodicity is in full agreement with the new interlayer distance that appears in the PXRD pattern (see above), which dismisses the idea that 2.8 nm height is related to $MnPS_3$ trilayer stacked units homogenously obtained by the exfoliation procedure.[27] From our point of view, this result can be better understood by picturing the exfoliated material as a hybrid system of single $MnPS_3$ flakes sandwiched in between tight

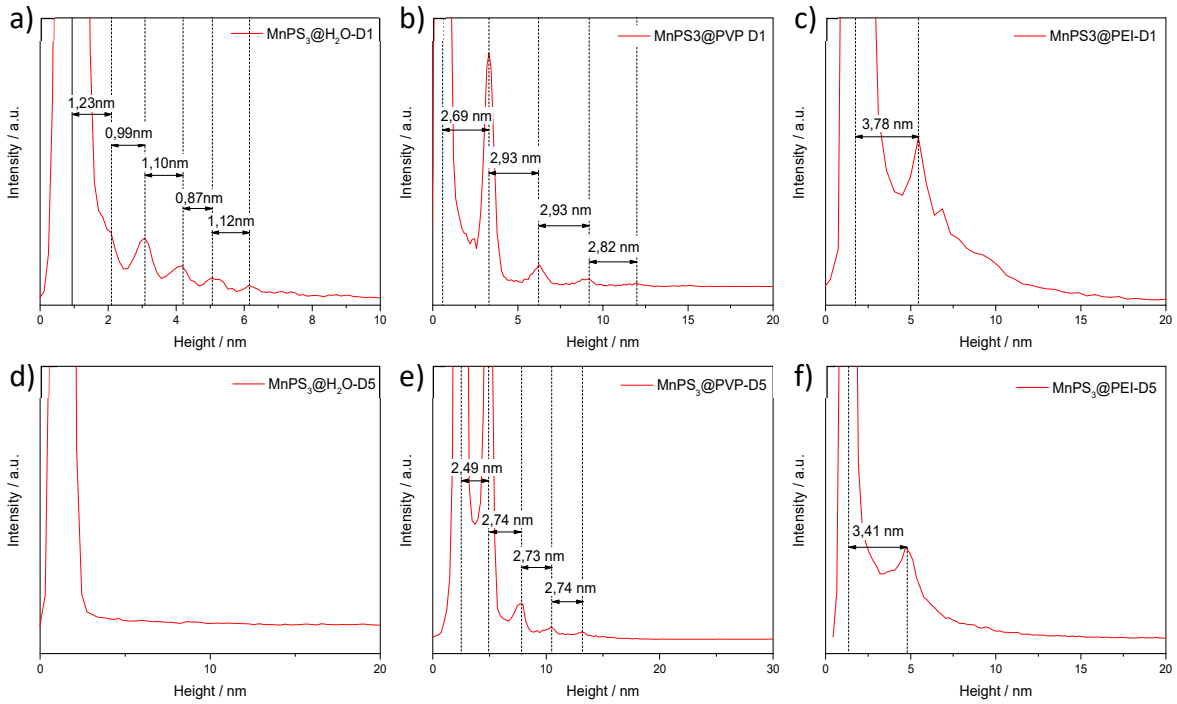

Fig. 3 Height histograms of AFM images presented in Fig. S9. Top: $MnPS_3@H_2O$ (a), $MnPS_3$@PVP (b) and $MnPS_3$@PEI (c) spin-coated on Si/SiO_2 substrates right after suspensions were prepared (day 1). Bottom: $MnPS_3@H_2O$ (d), $MnPS_3$@PVP (e) and $MnPS_3$@PEI (f) spin-coated on Si/SiO_2 substrates five days after suspensions, used in top histograms, were prepared (day 5).

homogeneous layers of polymer (ESI Scheme S1). Focusing now on $MnPS_3$@PEI, this composite gives a broad maximum in the histogram around 3.8 nm with no periodicity and a peak in the PXRD pattern corresponding to a new interlayer spacing of 1.14 nm. This points out to a smaller amount of polymer between the inorganic layers than in $MnPS_3$@PVP. This discrepancy between PXRD and AFM results may be due to the formation of a few-layer material when deposited on substrates for AFM studies.

Additionally, the stability of the three suspensions was evaluated by depositing the flakes on Si/SiO_2 substrates at different days since the suspensions of exfoliated matrials were prepared. In Fig. 4(d-f) we see that after 5 days, there are no flakes in the $MnPS_3@H_2O$ sample. In contrast, the samples covered by a polymer are stable for days (or even weeks, ESI Fig. S12). Thus, after 35 days, we have been capable of measuring flakes with the same size and shape as the first day, suggesting that the tight polymeric layer keeps the flakes isolated in solution and prevents further restacking. Therefore, if we want to preserve a stable ink of $MnPS_3$ flakes, the presence of a capping agent is mandatory. In contrast, if bare flakes are requested for a specific application, it is desirable to use freshly prepared suspensions.

Electrochemistry

In order to evaluate the quality and applicability of our exfoliated materials, we decided to study their electrocatalytic performance. $MnPS_3$ has been previously used as a catalyst for water splitting,[28] and its efficiency towards hydrogen evolution reaction (HER) has been demonstrated to increase when exfoliated.[15] However, in this report, the exfoliation procedure was not assisted through chemical intercalation and, as a result, the flakes were of lower morphological quality than those reported in the present work.

To test our exfoliated materials as HER catalysts, electrochemical measurements were performed in a three-electrode cell composed of platinum wire, Ag/AgCl and glassy carbon as counter, reference and working electrodes, respectively. The glassy carbon electrode was covered with bulk $MnPS_3$, $MnPS_3@H_2O$, $MnPS_3$@PVP, or $MnPS_3$@PEI, depending on the system under study. The obtained linear sweep voltammetry (LSV) curves are shown in Fig. 6a, while the overpotentials (η) for an intensity of 10 and 20 $mA{\cdot}cm^{-2}$ are depicted in Fig. 6b. It is interesting to point out the significant decrease of η (absolute value), when the bulk material is exfoliated. The best results are performed by the $MnPS_3@H_2O$ system, since in this case a higher number of active sites are accessible to H_3O^+ ions obtaining a value of η which is ~300 mV lower than previously reported results.[15] Nevertheless, through AFM studies, we know that bare layers are not stable for long time in solutionand this could be a handicap for the use of this material in commercial catalytic applications.

To work with more stable suspensions, we need to rely on the use of capping agents. In the case of $MnPS_3$@PVP the increase of the catalytic activity is very mild in comparison to the bulk. This observation is the result of two opposite effects: On the one hand, the exfoliation of $MnPS_3$ gives rise to a higher number of layers in contact with hydronium ions, therefore increasing catalytic active

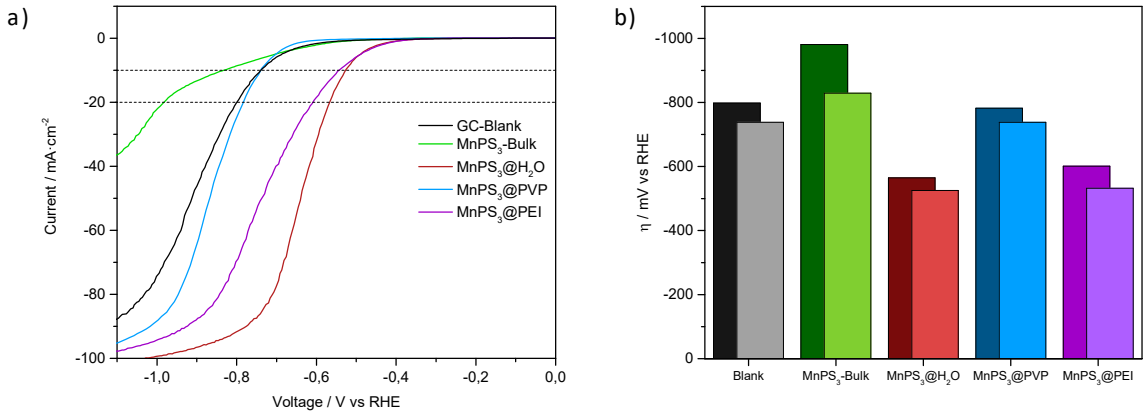

Fig. 4 a) Linear sweep voltammetry curves of bulk $MnPS_3$ (green), $MnPS_3@H_2O$ (red), $MnPS_3$@PVP (blue) and $MnPS_3$@PEI (purple) as powder deposited on the glassy carbon working electrode. Black curve corresponds to the blank experiment with a bare glassy carbon working electrode. b) overpotential values for current densities of 10 (light colour) and 20 (dark colour) $mA{\cdot}cm^{-2}$ extracted from (a), for bulk $MnPS_3$ (green), $MnPS_3@H_2O$ (red), $MnPS_3$@PVP (blue), $MnPS_3$@PEI (purple) and bare glassy carbon (black).

site. On the other hand, the layers are covered by a tight layer of PVP, with an intense interaction with metallic centres, that prevents the H_3O^+ ions from reaching the catalytic active sites and hence, decreases the catalytic efficiency dramatically. Therefore, this capping agent, despite providing a good exfoliation yield, and stable suspensions, is not suitable for this catalytic applications. Finally, with the $MnPS_3$@PEI system, we find a result that fulfills both criteria: It is stable for long time in solution (as indicated by AFM) and has a high catalytic performance. The reason for this interesting result may be related to the structure of PEI, much less dense and packed than the PVP one, allowing the access of H_3O^+ ions to the layers. At the same time, it is tight enough for preventing the restacking of $MnPS_3$ layers with time. In fact, PEI capping agent has been used previously for catalysis-related applications of nanomaterials.[22]

In order to compare our results with the ones obtained in the literature, all previous measurements have been performed in acidic media and using a platinum wire as the counter electrode. However, knowing that some platinum contamination may happen with this system,[29] we have repeated the measurements using a graphite rod instead of platinum as a counter electrode, as some works suggest.[30] The overpotential values are much higher with this configuration, but the tendency among the four systems is the same, being the best catalyst $MnPS_3@H_2O$, followed by $MnPS_3$@PEI, $MnPS_3$@PVP, and bulk $MnPS_3$ (ESI Fig S13). This confirms the higher availability of electrocatalytic active sites in bare flakes and in those covered with PEI, in comparison with those covered with PVP.

Conclusions

In this work, we have shown that by a simple chemically exfoliation protocol, $MnPS_3$ can be effectively delaminated into single layers without the requirement of a capping agent. This result represents the preparation of aqueous suspensions of large-area high-quality flakes, which permit a high accessibility to their surfaces. These features boost the reactivity of these flakes in catalytic applications and opens the possibility of a subsequent molecular functionalization that could give rise to the development of a plethora of multifunctional materials that can be explored in the next future. Concurrently, if it is required to preserve the stability of the flakes in suspension, the use of capping agents is mandatory. We have proved how PVP, as well as PEI, can successfully stabilize $MnPS_3$ flakes in solution for several days. IR spectroscopy points out a strong interaction between the organic and inorganic counterparts that is significantly larger for PEI than for PVP, probably due to the interactions established between the amino groups of the polymer and S atoms of $MnPS_3$.

As proof of concept of the quality of the exfoliated systems, we have tested their performance as electrocatalysts for HER. These measurements highlight the improved efficiency of the exfoliated system compared to the bulk and reveal that PEI capping agent is an excellent option to reach a compromise between catalytic efficiency and suspension stability, thanks to the relative accessibility to the actives site on the $MnPS_3$ flakes, while avoiding restacking and precipitation.

Experimental

Materials

All chemicals involved in the solid chemistry synthesis, chemical exfoliation and capping of $MnPS_3$, are commercially available and were used as received without further purification. Mn (>99.9%), P (>99.99%), S (>99.998%), KCl (>99.0%), PVP (Mw ~55.000) and PEI, branched (Mw ~25.000) were purchased from Sigma Aldrich. LiCl (Anhydrous 99%) was purchased from Alfa Aesar.

$MnPS_3$ Synthesis

$MnPS_3$ powder was obtained by a solid-state reaction. Stoichiometric amounts of Mn, P and S powder were mixed, pressed into a pellet and made react as in previous works.[2] The obtained material was ground into a fine powder for characterization and further use.

$MnPS_3$ Intercalation and Exfoliation

$MnPS_3$ powder was used as obtained from the solid reaction and grinding procedure. The exfoliation process was based in already-reported works of intercalation [17] and exfoliation [18] of $MnPS_3$ plus a sonication step with probe sonicator.

In this procedure 300 mg of $MnPS_3$ powder was mixed with 25 mL of 3 M KCl aqueous solution and let stirring for 1 hour. The second step was centrifuging the mixture for removing the excess of K^+ ions. Then, the solid was collected, mixed with 20 mL of 2 M LiCl aqueous solution and let stirring overnight.

After the intercalation steps, the suspension was sonicated in a probe sonicator during 20 minutes with 20% of amplitude and pulsed sonication of 6s on 2s off. Finally, a centrifuge step was performed for removing the Li^+ ions and the sample was resuspended in water, a second washing step was performed by centrifugation and the precipitate was resuspended in water or in aqueous solutions with different capping agents (PVP, PEI) with a 10 g/L concentration. Finally, the excess of capping agent was removed by three successive centrifugation steps for 30 minutes at 13.400 rpm.

Structural and chemical characterization: The material obtained from the exfoliation steps was dried in vacuum overnight and grinded prior to its structural characterization. Infrared spectra were collected using an ALPHA II FTIR spectrometer (Bruker). XPS spectra were measured with a K-ALPHA Thermo Scientific equipment with an X-Ray source of Al Kα radiation (1486.6eV), monochromatized by a twin crystal monochromator. Thermogravimetric analyses were carried out with TGA 550 (TA Instruments) in high-resolution mode (Ramp: 20.0 °C/min from 25 °C to 700 °C) XRPD of the obtained material was measured at room temperature in an Empyrean PANalytical powder diffractometer using Cu K-α radiation (λ=1.5418 Å) and working on transmission mode. Raman spectra were collected with a Raman Emission Horiba-MTB Xplora Spectrometer with a 532 nm laser. Samples were prepared dropcasting suspensions on Si/SiO_2 substrates.

Morphological characterization: For the morphological characterization, $MnPS_3$ suspensions were deposited onto Si/SiO_2 substrates, for this purpose, 10 µL of suspension was dropped onto spinning substrates at 50rps for 60s. The morphology and thickness of flakes thus obtained were measured in Peak-Force Tapping mode with a Bruker Dimension ICON AFM .

Electrochemical characterization: LSV measurements were performed using a Gamry 1010 potentiostat with a three-electrode cell composed by Pt wire as counter electrode, Ag/AgCl as reference electrode and glassy carbon rotating electrode (Ø 3mm) as working electrode for the main measurements. Working electrodes were loaded with 10 µL of the target $MnPS_3$ suspensions and let dry. For additional measurements (represented in SI) a graphite rod was used as a counter electrode instead of Pt wire and LSV curves were recorded in the same way. H_2SO_4 0.5 M was used as electrolyte in all cases and was purged with N_2 bubbling prior to measurements.

Author Contributions

We strongly encourage authors to include author contributions and recommend using CRediT for standardised contribution descriptions. Please refer to our general author guidelines for more information about authorship.

Conflicts of interest

There are no conflict of interest to declare.

Acknowledgements

The authors acknowledge the financial support from the EU (ERC-Advanced Grant 78822-MOL-2D, and FET-OPEN COSMICS 766726,), the Spanish MICINN (PID2020-117264GB-I00; PID2020-117152RB-I00; Excellence Unit María de Maeztu CEX2019-000919-M; and EQC2019-006517-P and EQC2019-005816-P, cofinanced by FEDER), and the Generalitat Valenciana (Prometeo Program of Excellence: PROMETEO/2017/066; PO FEDER Program: IDIFEDER/2020/063). I.B.-A. (FPU18/00432) and M.M.-G. thanks the Spanish MICINN for the award of FPU Grants.

References

1 M. A. Susner, M. Chyasnavichyus, M. A. McGuire, P. Ganesh and P. Maksymovych, *Adv. Mater.*, 2017, **29**, 1–39.

2 M. Šiškins, M. Lee, S. Mañas-Valero, E. Coronado, Y. M. Blanter, H. S. J. van der Zant and P. G. Steeneken, *Nat. Commun.*, 2020, **11**, 2698.

3 D. Afanasiev, J. R. Hortensius, M. Matthiesen, S. Mañas-Valero, M. Šiškins, M. Lee, E. Lesne, H. S. J. van der Zant, P. G. Steeneken, B. A. Ivanov, E. Coronado and A. D. Caviglia, *Sci. Adv.*, 2021, **7**, eabf 3096.

4 R. Brec, D. M. Schleich, G. Ouvrard, A. Louisy and J. Rouxel, *Inorg. Chem.*, 1979, **18**, 1814–1818.
5 M. Ramos, F. Carrascoso, R. Frisenda, P. Gant, S. Mañas-Valero, D. L. Esteras, J. J. Baldoví, E. Coronado, A. Castellanos-Gomez and M. R. Calvo, *npj 2D Mater. Appl.*, , DOI:10.1038/s41699-021-00199-z.
6 B. L. Chittari, Y. Park, D. Lee, M. Han, A. H. Macdonald, E. Hwang and J. Jung, *Phys. Rev. B*, 2016, **94**, 1–16.
7 G. Long, H. Henck, M. Gibertini, D. Dumcenco, Z. Wang, T. Taniguchi, K. Watanabe, E. Giannini and A. F. Morpurgo, *Nano Lett.*, 2020, **20**, 2452–2459.
8 G. Long, T. Zhang, X. Cai, J. Hu, C. W. Cho, S. Xu, J. Shen, Z. Wu, T. Han, J. Lin, J. Wang, Y. Cai, R. Lortz, Z. Mao and N. Wang, *ACS Nano*, 2017, **11**, 11330–11336.
9 C. C. Mayorga-Martinez, Z. Sofer, D. Sedmidubský, Š. Huber, A. Y. S. Eng and M. Pumera, *ACS Appl. Mater. Interfaces*, 2017, **9**, 12563–12573.
10 F. Kargar, E. A. Coleman, S. Ghosh, J. Lee, M. J. Gomez, Y. Liu, A. S. Magana, Z. Barani, A. Mohammadzadeh, B. Debnath, R. B. Wilson, R. K. Lake and A. A. Balandin, *ACS Nano*, 2020, **14**, 2424–2435.
11 T. A. Shifa, F. Wang, Z. Cheng, P. He, Y. Liu, C. Jiang, Z. Wang and J. He, *Adv. Funct. Mater.*, 2018, **28**, 1800548.
12 H. Zhang, T. Yi, F. Li, E. Delahaye, P. Yu and R. Clement, *J. Photochem. Photobiol. A Chem.*, 2007, **186**, 173–177.
13 V. Nicolosi, M. Chhowalla, M. G. Kanatzidis, M. S. Strano and J. N. Coleman, *Science*, 2013, **340**, 72–75.
14 F. Bonaccorso, A. Bartolotta, J. N. Coleman and C. Backes, *Adv. Mater.*, 2016, **28**, 6136–6166.
15 R. Gusmão, Z. Sofer and M. Pumera, *Adv. Funct. Mater.*, 2018, **29**, 1805975.
16 R. Kumar, R. N. Jenjeti and S. Sampath, *Adv. Mater. Interfaces*, 2019, **6**, 1–8.
17 I. Lagadic, P. G. Lacroix and R. Clément, *Chem. Mater.*, 1997, **9**, 2004–2012.
18 R. F. Frindt, D. Yang and P. Westreich, *J. Mater. Res.*, 2004, **20**, 1107–1112.
19 L. M. Rossi, J. L. Fiorio, M. A. S. Garcia and C. P. Ferraz, *Dalt. Trans.*, 2018, **47**, 5889–5915.
20 Z. Niu and Y. Li, *Chem. Mater.*, 2014, **26**, 72–83.
21 K. M. Koczkur, S. Mourdikoudis, L. Polavarapu and S. E. Skrabalak, *Dalt. Trans.*, 2015, **44**, 17883–17905.
22 L. Bai, H. Zhu, J. S. Thrasher and S. C. Street, *ACS Appl. Mater. Interfaces*, 2009, **1**, 2304–2311.
23 M. Liu, X. Yan, H. Liu and W. Yu, *React. Funct. Polym.*, 2000, **44**, 55–64.
24 X. Zhang, H. Zhou, X. Su, X. Chen, C. Yang, J. Qin and M. Inokuchi, *J. Alloys Compd.*, 2007, **432**, 247–252.
25 H. Liu, T. Kuila, N. H. Kim, B. C. Ku and J. H. Lee, *J. Mater. Chem. A*, 2013, **1**, 3739–3746.
26 D. Yang and R. F. Frindt, *J. Mater. Res.*, 2000, **15**, 2408–2413.
27 W. Bai, Z. Hu, C. Xiao, J. Guo, Z. Li, Y. Zou, X. Liu, J. Zhao, W. Tong, W. Yan, Z. Qu, B. Ye and Y. Xie, *J. Am. Chem. Soc.*, 2020, **142**, 10849–10855.
28 C. C. Mayorga-Martinez, Z. Sofer, D. Sedmidubský, Š. Huber, A. Y. S. Eng and M. Pumera, *ACS Appl. Mater. Interfaces*, 2017, **9**, 12563–12573.
29 D. Voiry, M. Chhowalla, Y. Gogotsi, N. A. Kotov, Y. Li, R. M. Penner, R. E. Schaak and P. S. Weiss, *ACS Nano*, 2018, **12**, 9635–9638.
30 R. Wei, M. Fang, G. Dong and J. C. Ho, *Sci. Bull.*, 2017, **62**, 971–973.

Molecular stabilization of chemically exfoliated bare $MnPS_3$ layers

Isaac Brotons-Alcázar,[a] Ramón Torres-Cavanillas[a] Marc Morant-Giner[a], Samuel Mañas-Valero[a], Alicia Forment-Aliaga*[a] and Eugenio Coronado.*[a]

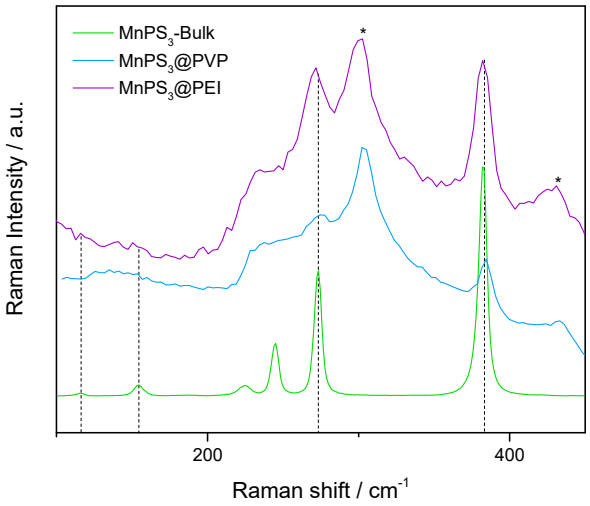

Fig. S1.- Raman spectra of bulk $MnPS_3$, $MnPS_3$@PVP and $MnPS_3$@PEI. Substrate-related peaks are marked as *.

Raman spectra were collected by spin-coating suspensions of different $MnPS_3$-based systems onto Si/SiO_2 substrates. 532 nm laser was employed for performing the measurements.

Table S1.- Raman active modes for $MnPS_3$, $MnPS_3$@PVP and $MnPS_3$@PEI.

Vibration mode	**$MnPS_3$ Bulk**	**$MnPS_3$@PVP**	**$MnPS_3$@PEI**
B_g	115	-	116
A_g	154	-	151
A_g, B_g	224	238	235
A_g	245		
A_g, B_g	274	275	275
Si-O	-	304	303
A_g	383	385	383
Si	-	433	432

In **Fig. S2** the main bands of PVP are highlighted pointing out the good agreement of bare PVP bands and those in $MnPS_3$@PVP system. The carbonyl band is shifted to lower energies in the $MnPS_3$@PVP system.

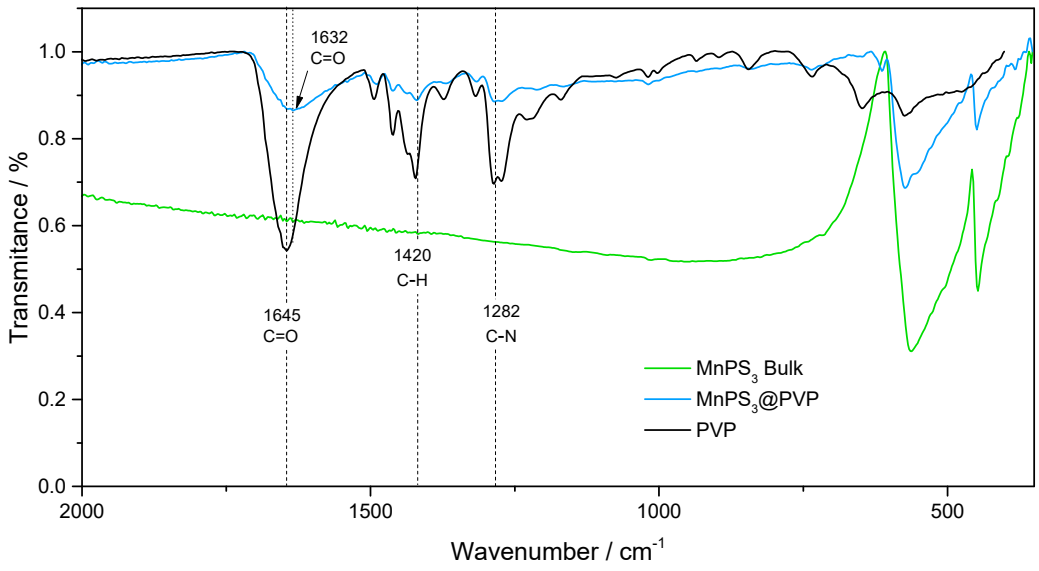

Fig. S2.- Infrared spectra of bulk $MnPS_3$; $MnPS_3$@PVP and commercial PVP

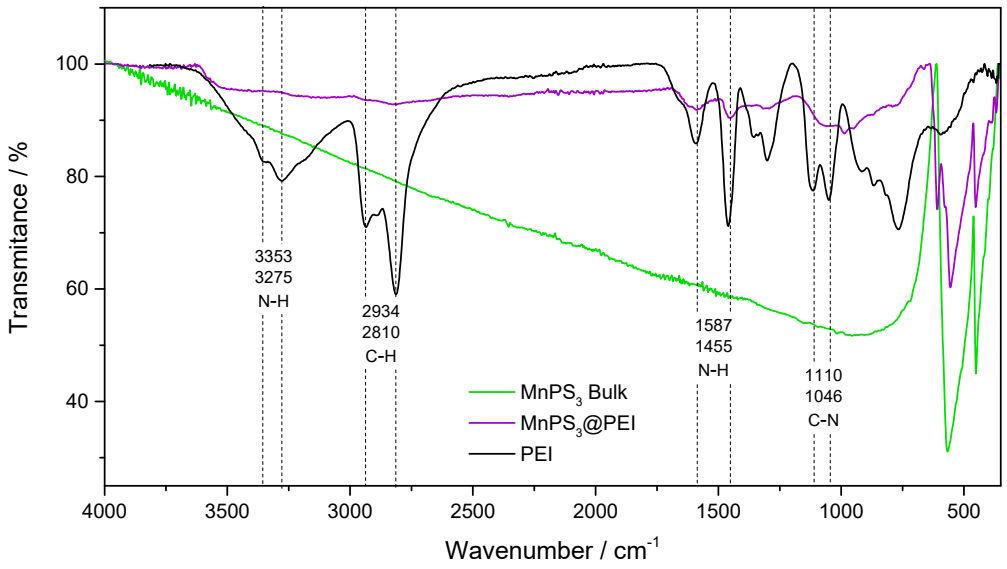

Fig. S3.-Infrared spectra of bulk $MnPS_3$; $MnPS_3$@PEI and commercial PEI

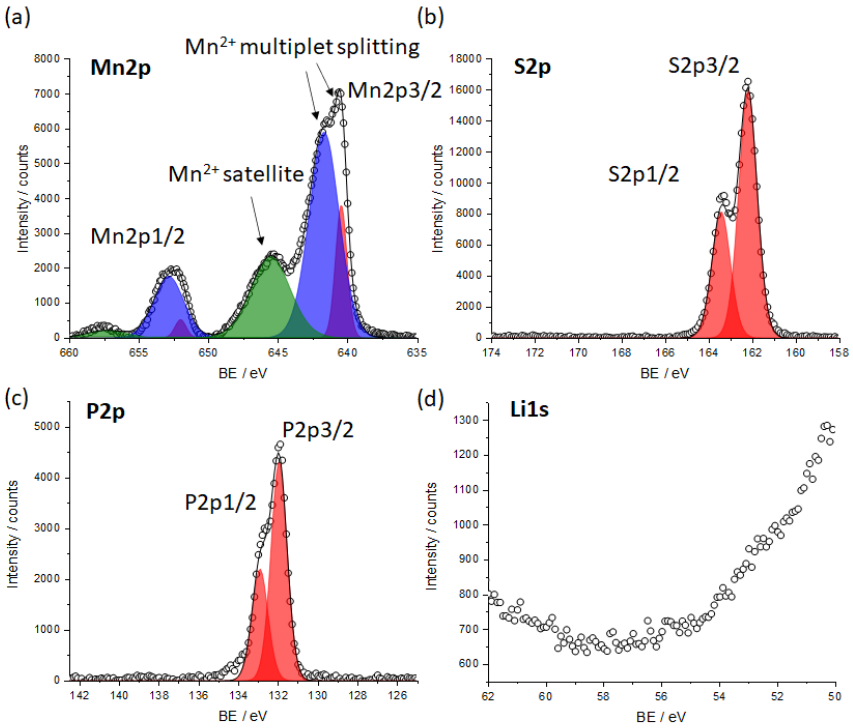

Fig. S4.- a) Mn 2p, b) S2p, c)P2p, and d) Li1s XPS regions of $MnPS_3$@H_2O. Representation of the main peaks (red) (and blue, for Mn splitting) and satellite peaks (green).

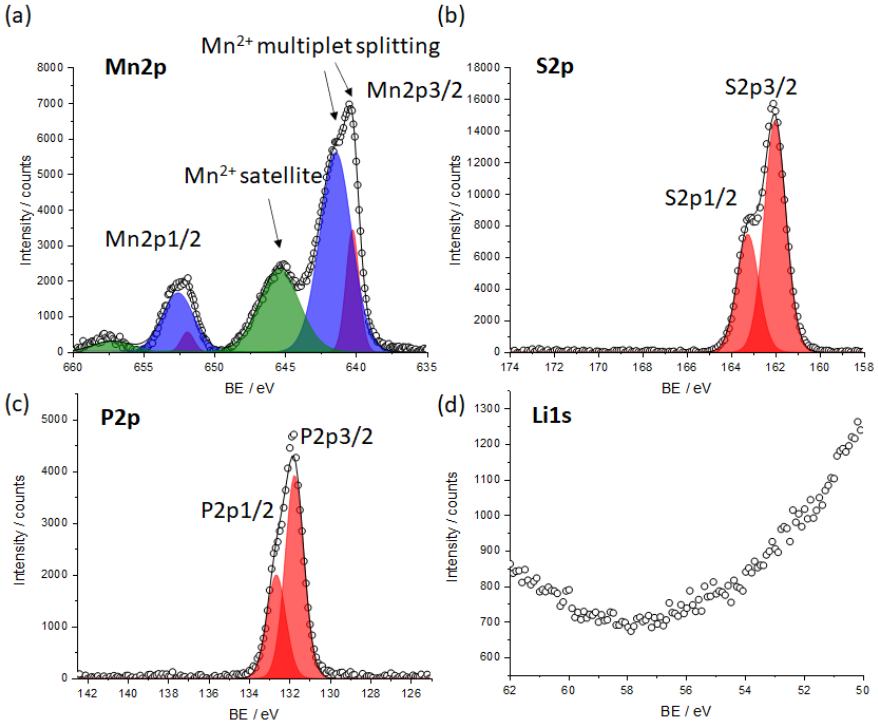

Fig. S5.-a) Mn 2p, b) S2p, c)P2p, and d) Li1s XPS regions of $MnPS_3$@PVP. Representation of the main peaks (red) (and blue, for Mn splitting) and satellite peaks (green).

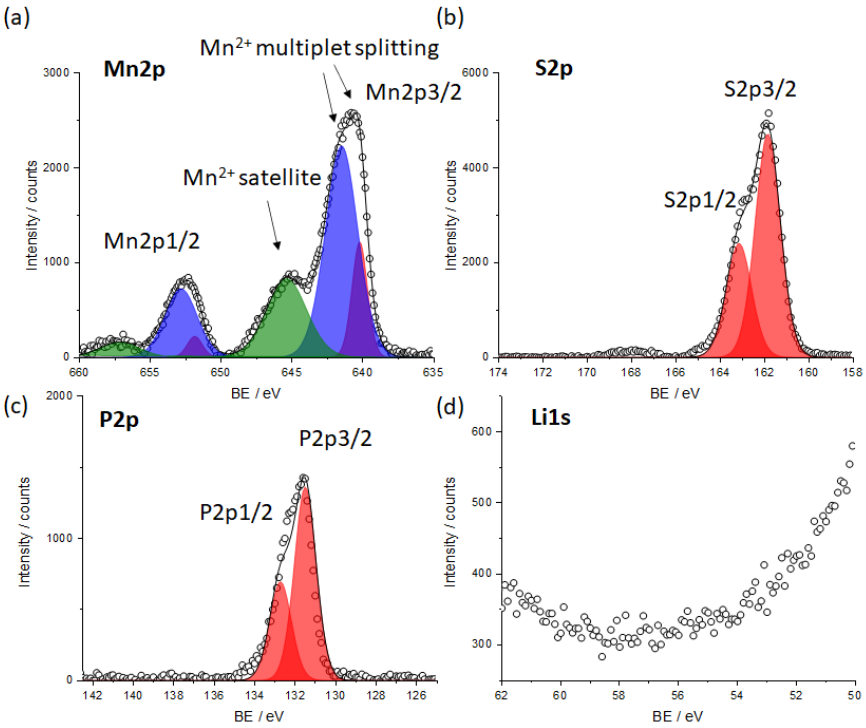

Fig. S6.- a) Mn 2p, b) S2p, c)P2p, and d) Li1s XPS regions of $MnPS_3$@PEI. Representation of the main peaks (red) (and blue, for Mn splitting) and satellite peaks (green).

The electronic signature of the exfoliated material exhibits a complex Mn2p region due to significant multiplet splitting and satellite peaks, Fig S4-S6 (a).[1,2] For all the samples, two sets of bands around 641 eV and 652 eV can be observed, corresponding to the $Mn2p_{3/2}$ and $Mn2p_{1/2}$ levels of Mn^{2+}. For simplicity, each set of bands has been deconvoluted in two main peaks and a satellite.

Also, the presence of S and P is evidenced for the different samples by the appearance of the characteristic S2p and P2p doublets (Fig S4-S6 b and c), while no residual Li^+ from the exfoliation protocol is recorded (Fig S4-S6 d).

Remarkably, the ratio Mn:P:S of the three samples can be quantified from the XPS, estimating values close to the expected 1:1:3 (Table S2), indicating negligible amount of Mn vacancies.

Table S2.- Mn:P:S atomic ratio for $MnPS_3@H_2O$, $MnPS_3$@PVP and $MnPS_3$@PEI

Sample	Ratio Mn:P:S
$MnPS_3@H_2O$	0.9:1.0:2.8
$MnPS_3$@PVP	1.0:1.0:2.9
$MnPS_3$@PEI	1.0:1.0:2.9

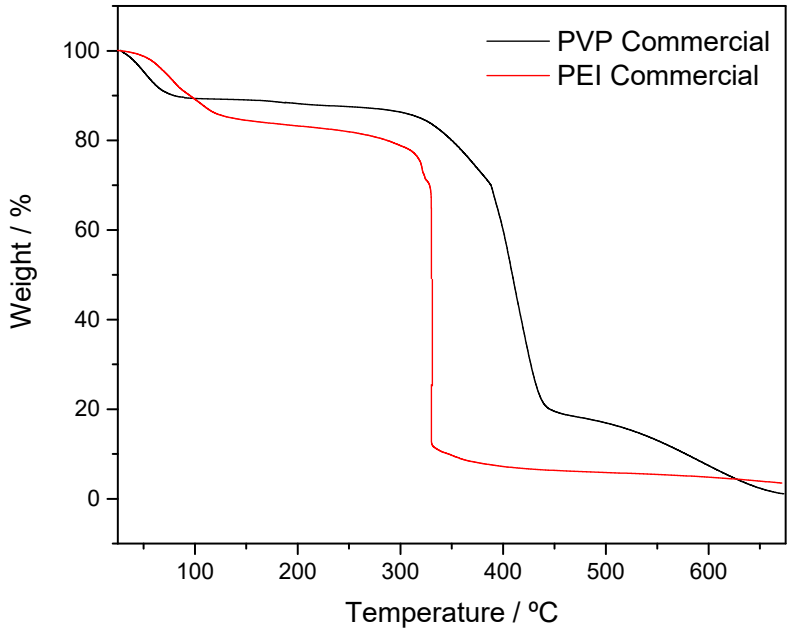

Fig. S7.- TGA analysis under N_2 atmosphere of PVP (Black) and PEI (Red)

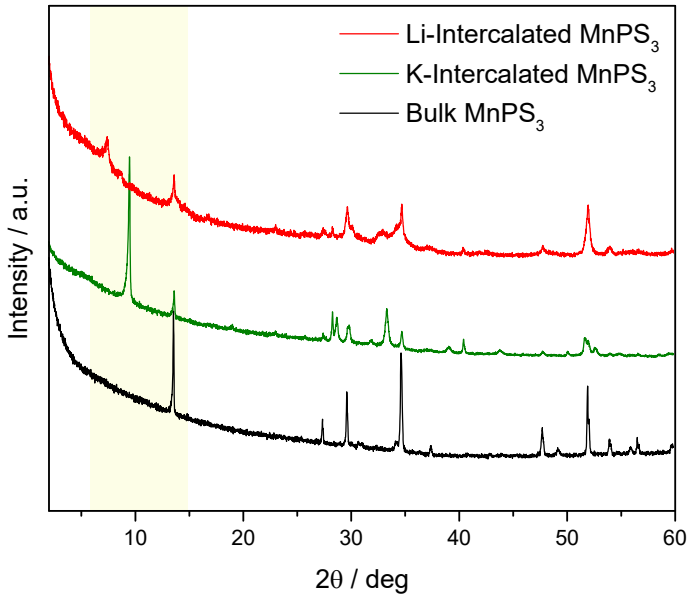

Fig. S8.- XRPD of bulk $MnPS_3$ (Black), K-intercalated $MnPS_3$ (Green) and Li-intercalated $MnPS_3$ (Red). Highlighted area corresponds to the (001) peak displacement.

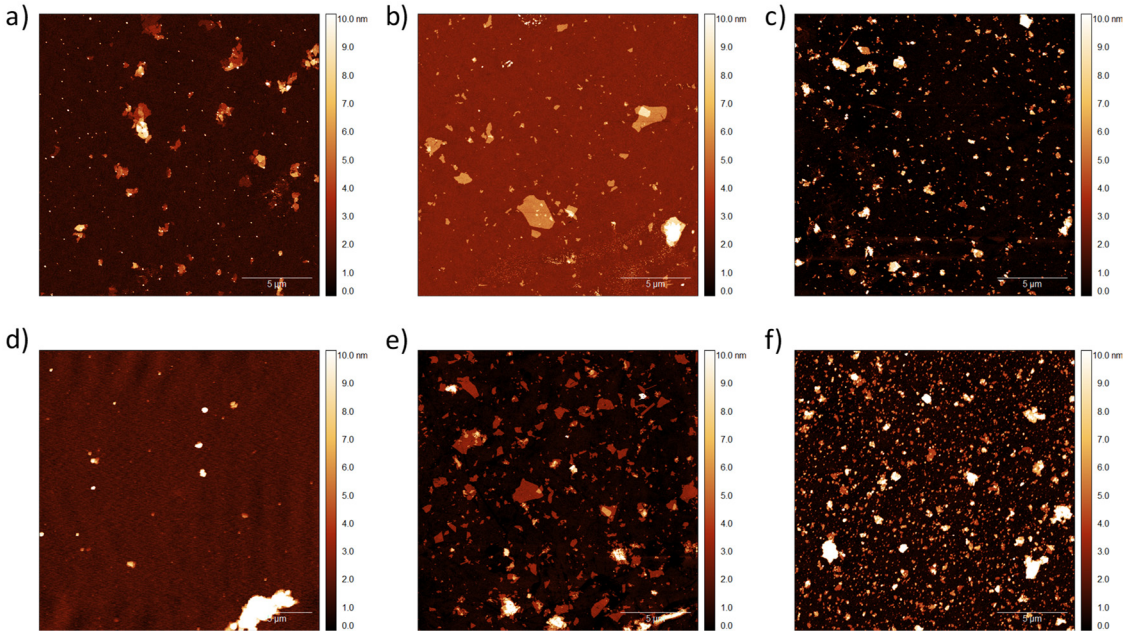

Fig. S9.- Full 20x20 µm^2 AFM topography images of $MnPS_3$@H_2O (a), $MnPS_3$@PVP (b) and $MnPS_3$@PEI (c) spin-coated on Si/SiO_2 substrates right after suspensions were prepared (day 1). Bottom: AFM topography images of $MnPS_3$@H_2O (a), $MnPS_3$@PVP (b) and $MnPS_3$@PEI (c) spin-coated on Si/SiO_2 substrates five days after suspensions used in top images, were prepared (day 5). These images correspond to bigger scope of Fig 5 (a)-(f).

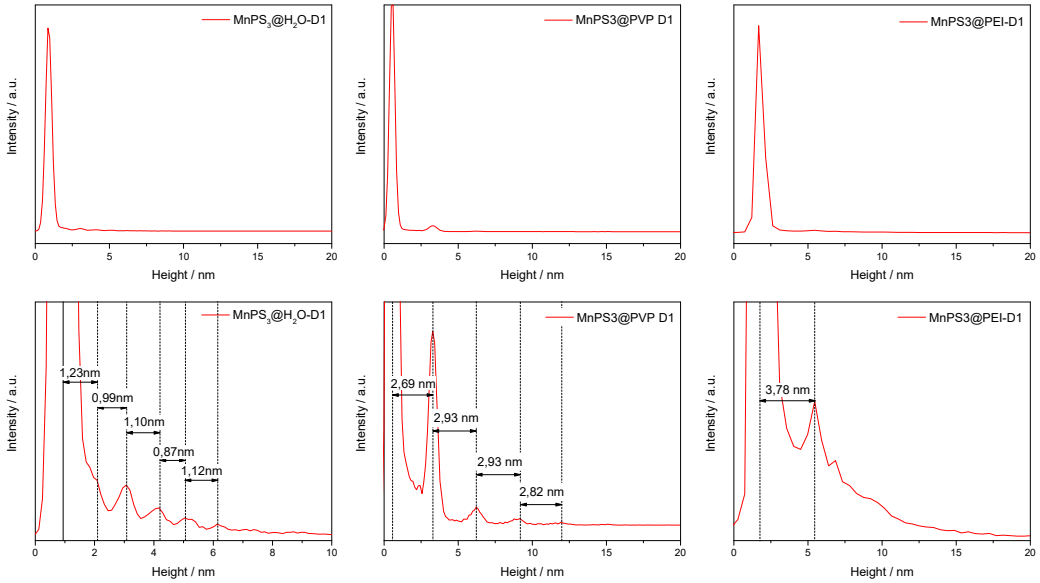

Fig. S10.- Height histograms of first-day samples of a)$MnPS_3@H_2O$, b)$MnPS_3$@PVP and c)$MnPS_3$@PEI; d), e) and f) are onsets of a), b) and c), respectively. Histograms (a), (b) and (c) correspond to the pictures presented in Fig S9 (a), (b) and (c).

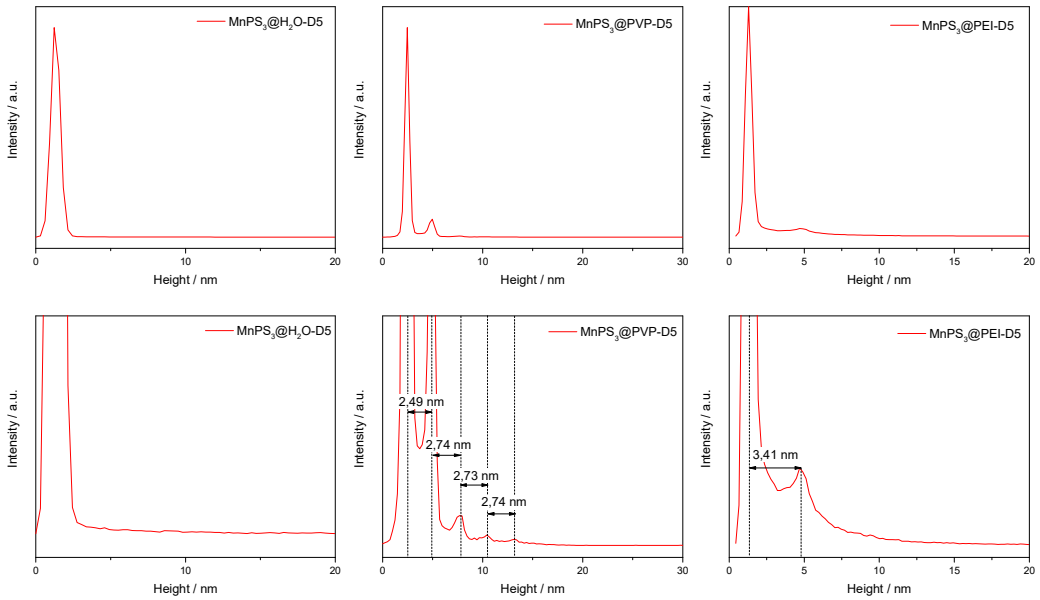

Fig. S11.- Height histograms of fifth-day samples of a)$MnPS_3@H_2O$, b)$MnPS_3$@PVP and c)$MnPS_3$@PEI; d), e) and f) are onsets of a), b) and c), respectively. Histograms (a), (b) and (c) correspond to the pictures presented in Fig S9 (d), (e) and (f)

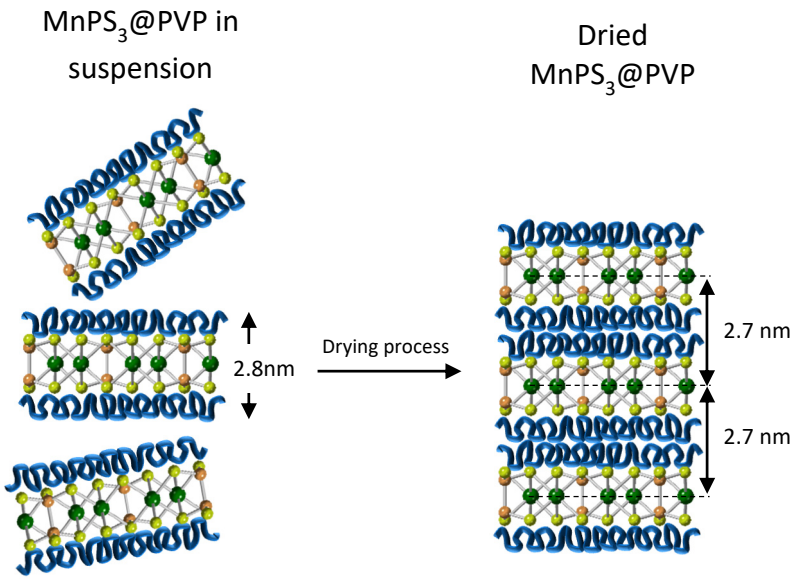

Scheme S1.- Proposed arrangement for $MnPS_3$@PVP layers in suspension and in dried form. Layer thickness determined by AFM (a) and layered structure deduced by XRD (b).

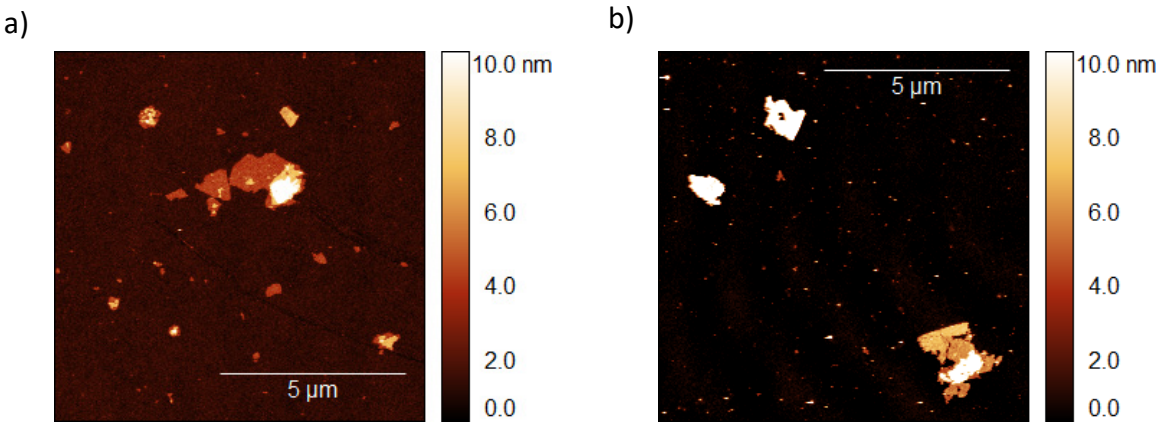

Figure S12.- AFM images taken 35 days after exfoliation of $MnPS_3$@PVP (a) and $MnPS_3$@PEI (b)

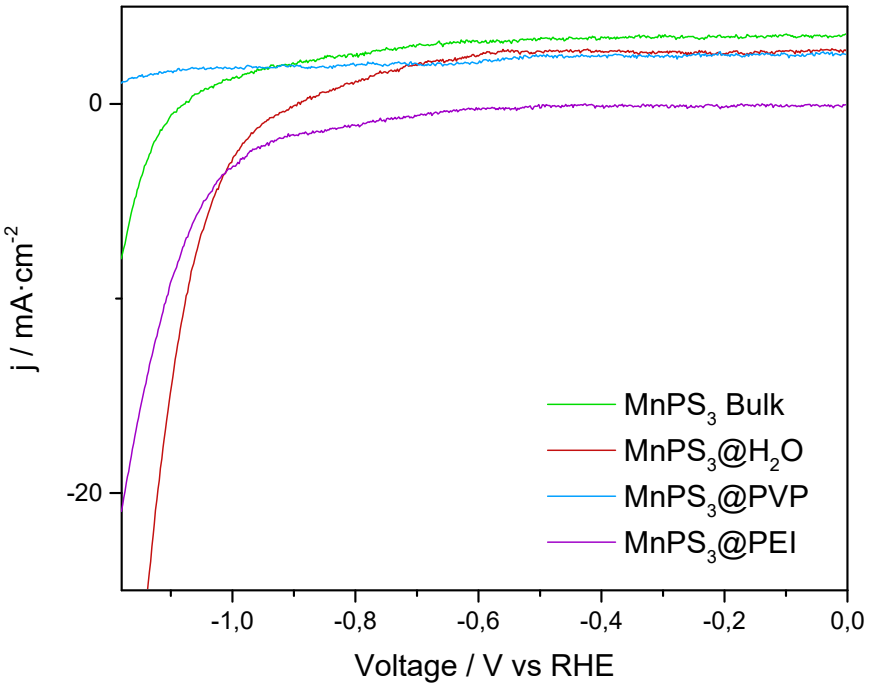

Fig. S13.- LSV measurements for bulk $MnPS_3$, $MnPS_3@H_2O$, $MnPS_3$@PVP and $MnPS_3$@PEI deposited onto glassy carbon working electrode.

All the $MnPS_3$ systems were measured using an electrochemical cell with graphite rod as counter electrode, Ag/AgCl as reference electrode and glassy carbon covered with the target $MnPS_3$ system as working electrode. With this system the values of current density are much lower than the platinum-based system, however, for the sake of comparison, it is worth noting how the tendency of catalytic performance is the same in both systems (Table SI3).

Table S3.- Overpotential values for current densities of 10 and 20 $mA{\cdot}cm^{-2}$ for bulk $MnPS_3$, $MnPS_3@H_2O$, $MnPS_3$@PVP and $MnPS_3$@PEI measured with platinum wire or graphite rod as counter electrode

	Pt as counter electrode		Graphite Rod as counter electrode	
	η@10mA·cm^{-2} /mV	η@20mA·cm^{-2} /mV	η@10mA·cm^{-2} /mV	η@20mA·cm^{-2} /mV
$MnPS_3$ Bulk	-829	-981	-	-
$MnPS_3@H_2O$	-525	-565	-1070	-1120
$MnPS_3$@PVP	-738	-782	-	-
$MnPS_3$@PEI	-532	-601	-1110	-1170